Anisotropic membrane curvature sensing by amphipathic peptides – supporting material

Jordi Gómez-Llobregat, Federico Elías-Wolff, Martin Lindén.
November 16, 2015

S1 Convergence and individual replicas

Simulations of proteins interacting with mixed bilayers can be challenging to converge due to slow lipid diffusion and long-lived protein-lipid interactions (1). For this reason, we run three independent replicas rather than one long simulation for each peptide, and use them as a simple control of the robustness of our conclusions. Figures S1-S3 show histograms of center-of-mass positions, orientations, and joint positions-orientations of both the three individual production runs for each peptide, as well as aggregated histograms. In the case of melittin (Fig. S2), orientations of both the N- and C-terminal helices are shown.

While the results for individual trajectories are obviously noisier than the aggregated statistics, it is clear that the same qualitative features are present in all replicas. In particular, two well-separated orientational states of melittin and LL-37 are clearly visible (albeit not equally populated) in all trajectories, strongly indicating that our simulations are long enough to capture the major low-energy states of these systems. However, the sampling is still limited enough to induce significant statistical uncertainty in fit parameters, as seen Fig. 4d.

S2 Location of the curvature sensing site on LL-37

LL-37 shows indications of asymmetry around $s = 0.5$ that is incompatible with the symmetry of the curvature tensor elements (Fig. 3d), and the fitted E_C model is also less consistent with the orientation averaged binding energy (Fig. 3e) than the other peptides. Here, we explore the hypothesis that these effects are caused by using the center-of-mass of the peptide for defining the position s, which might be inappropriate if the sensitivity is unequally distributed along the peptide. Our rationale for this hypothesis is that a correlation between position and orientation, as indicated in the LL-37 data in Fig. 3d might come about if the effective curvature sensing site is different than the center-of-mass which we tracked to extract that data, as sketched in Fig. 5.

In Fig. S4, we show the corresponding analysis for LL-37 assuming a few alternative effective curvature sensing sites, with the center-of-mass in the middle row. The correlation between θ and s around each peak clearly becomes more pronounced and N-terminal-like (c.f. Fig. 5) when the tracking site moves towards the N-terminal end. However, the asymmetry almost disappears when one assumes the effective curvature sensing site to be the

center of mass of the C-terminal helix, and appears again with the opposite C-terminal-like trend when tracking the C-terminal end. Of these cases, the center-of-mass of the C-terminal helix is most consistent with the symmetries of curvature tensor elements and thus acts as an effective "sensing site", which indicates that this part of the peptide is more important for curvature sensing. Fitting the E_C model to this data yields $\kappa = 323 \pm 127\ k_BT$nm, $C_0^{-1} = -4.1 \pm 0.5$ nm, $b = 8.2 \pm 0.6$ k$_B$Tnm, and $\alpha = 69 \pm 2°$, not significantly different from the parameters shown in Fig. 4.

However, all distributions are still slightly asymmetric around $s = 0.5$, with average s-values ranging from about 0.52 to 0.51 for the N- and C-terminal ends respectively, corresponding to an average displacement of 0.5 nm to 0.35 nm from the mid point. A closer examination of the significance of this observation would require substantially better statistics, perhaps from using some enhanced sampling method, as well as more systematic studies using a larger range of curvatures. This is outside the scope of this study.

Supporting references

1. Ge, C., J. Gómez-Llobregat, M. J. Skwark, J.-M. Ruysschaert, Å. Wieslander, and M. Lindén, 2014. Membrane remodeling capacity of a vesicle-inducing glycosyltransferase. *FEBS J.* 281:3667–3684.

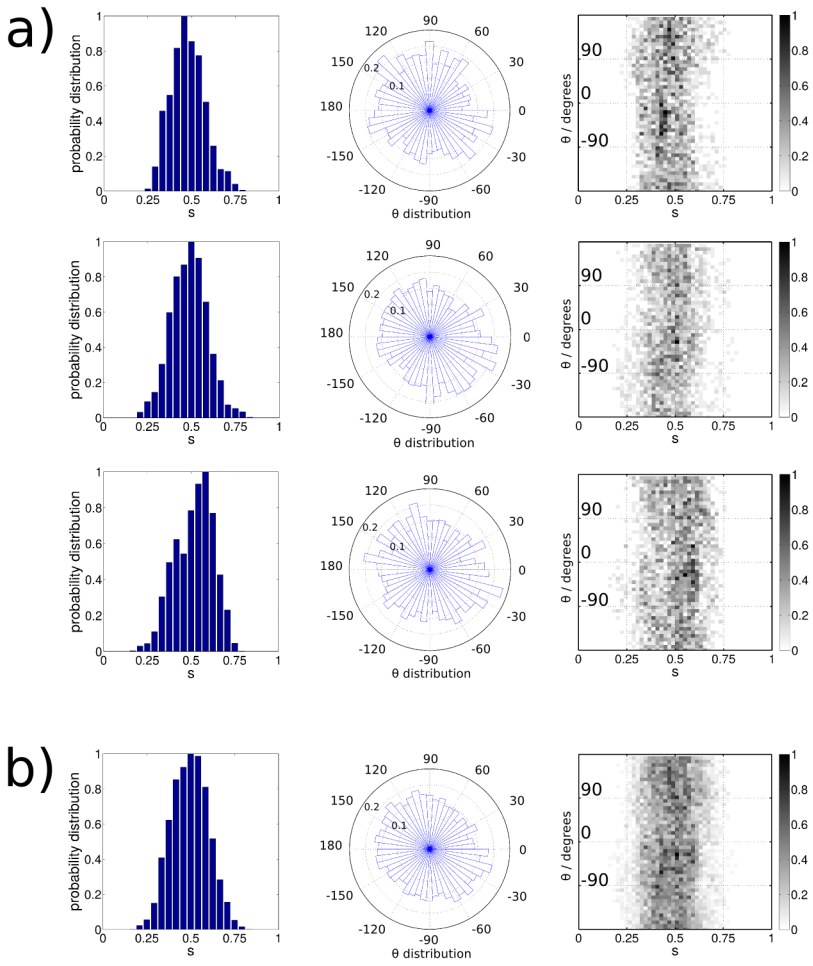

Figure S1: Results for magainin, from (a) three independent production runs, and (b) aggregated.

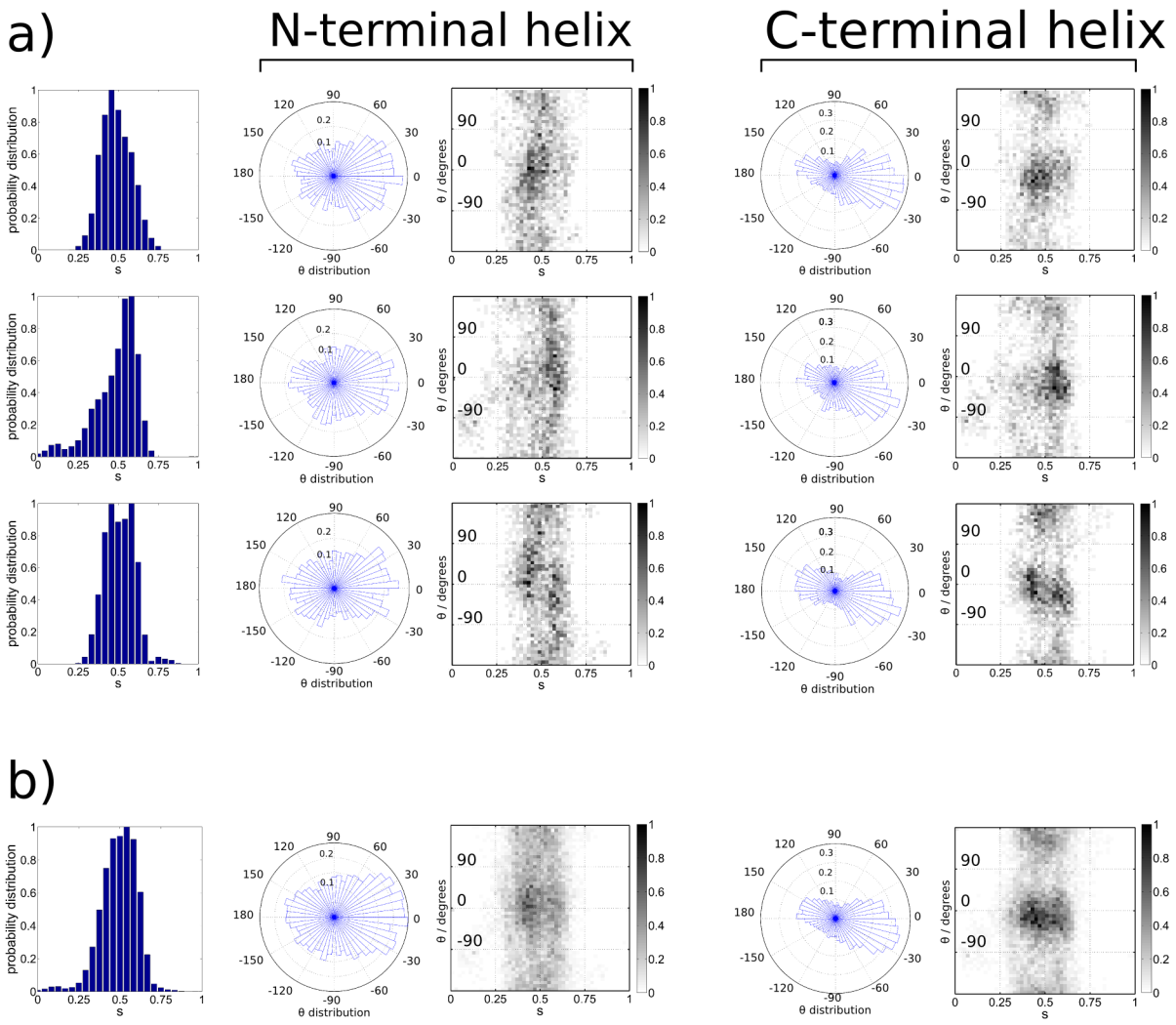

Figure S2: Results for melittin, from (a) the three independent production runs, and (b) aggregated. Both N- and C-terminal results are shown.

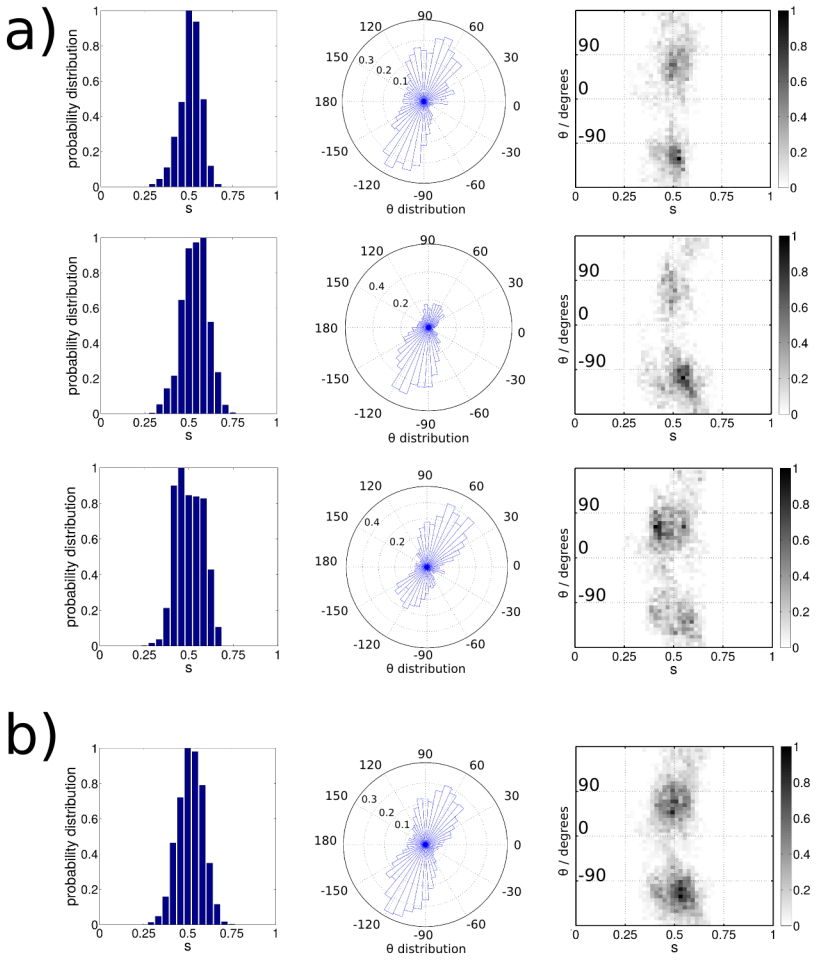

Figure S3: Results for LL-37, from (a) three independent production runs, and (b) aggregated.

Table S1: Fit parameters (fit± bootstrap std.) for the E_2 model for the curves shown in Fig. 4, rounded to two significant digits, in appropriate units of k_BT and nm. This model is given by

$$E_2 = \frac{a_1}{2}(C_\parallel - a_2)^2 + a_3(C_X - a_4)^2 + \frac{a_5}{2}(C_\perp - a_6)^2 + a_7 C_X(C_\parallel + C_\perp) + a_8 C_X(C_\parallel - C_\perp),$$

i.e., with a $C_\parallel C_\perp$-term omitted for identifiability.

	a_1	a_2	a_3	a_4
MAG	71 ± 30	-0.30 ± 0.26	73 ± 28	0.024 ± 0.028
MEL	170 ± 52	-0.23 ± 0.03	130 ± 52	0.002 ± 0.02
LL-37	300 ± 130	-0.24 ± 0.07	300 ± 140	-0.02 ± 0.03
	a_5	a_6	a_7	a_8
MAG	68 ± 28	-0.30 ± 0.27	-24 ± 19	5.3 ± 3.3
MEL	90 ± 55	-0.3 ± 1.3	27 ± 28	2.4 ± 4.2
LL-37	310 ± 150	-0.25 ± 0.73	68 ± 59	1 ± 7

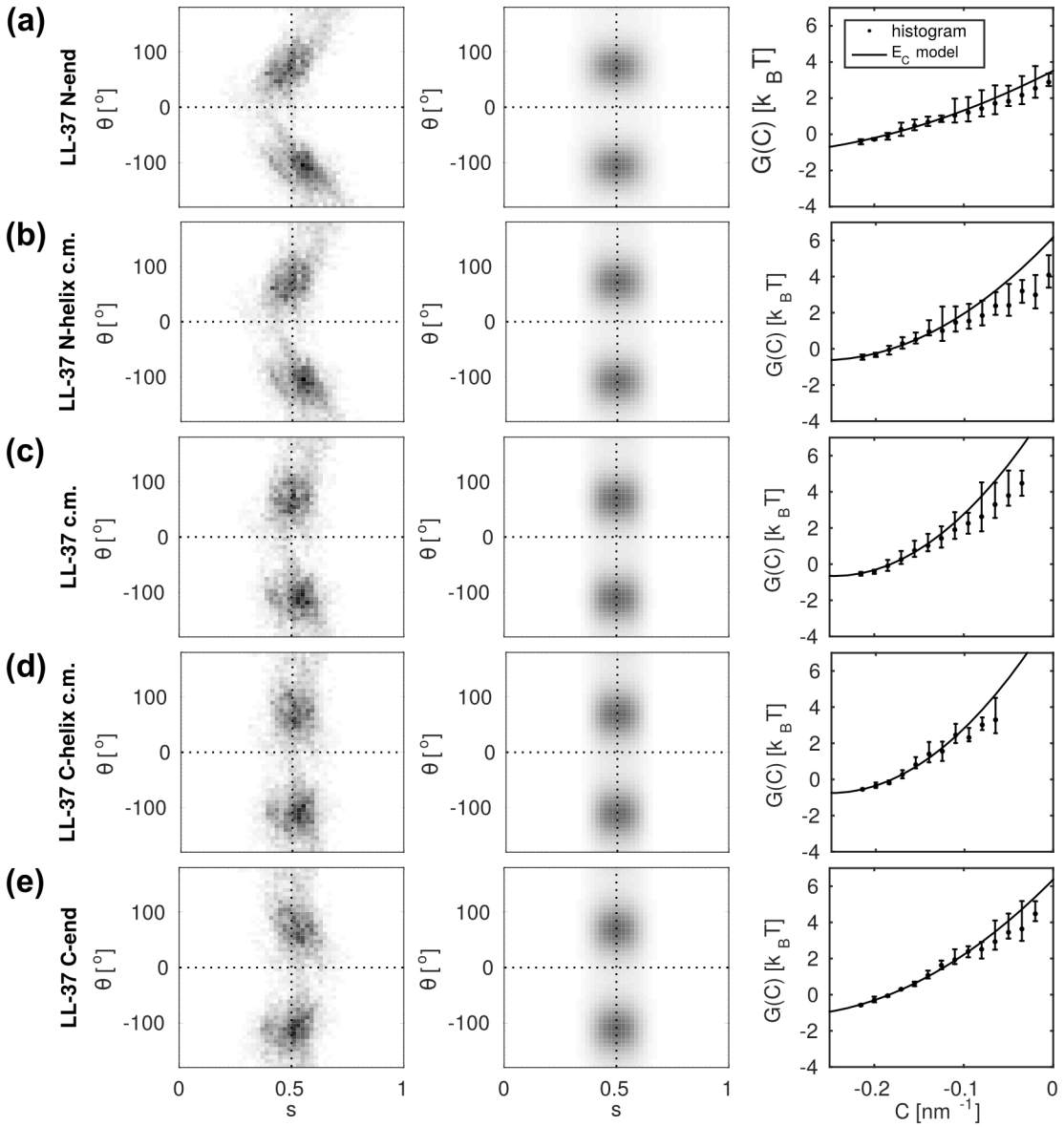

Figure S4: Analysis of LL-37 using different definitions of s and θ, namely (a) the first residue and orientation of the N-terminal helix, (b) the center-of-mass and orientation of the N-terminal helix, (c) the center-of-mass and orientation of the whole peptide (same as shown in the main text), (d) the center-of-mass and orientation of the C-terminal helix, and (e) the last residue and orientation of the C-terminal helix. relevant curvature sensing site. The columns show (left) the (s, θ)-histogram, (mid) a fit of the E_C model, and (right) the orientation-averaged binding free energy, obtained from the model fit (line) or using weighted histograms, Eq. 4, (dots) with error bars as in Fig. 3. The fit and histogram curves are vertically aligned by least-squares fit of the points at $C \leq -0.15$ nm^{-1}.